SECONDARY DAMAGE MODES IN LAMINATES INITIATED BY INTRALAMINAR CRACKS

Dionysios T. G. Katerelos and Janis Varna

Luleå University of Technology
SE 971 87, Luleå, Sweden
d.katerelos@gmail.com

ABSTRACT

Damage developing within laminated composites is a result of complex combinations of thermo-mechanical and environmental loads. Intralaminar (transverse) cracking is the first mode of damage appearing. The cracks act as stress concentration locations resulting in the development of additional damage modes. These modes include fibres breakage, matrix yielding, longitudinal splitting and local delaminations. The mode of damage that will grow depends on the laminate lay-up and local statistical strength of the layers and interfaces. In the present paper the stress state in the proximity of the transverse crack tip is investigated in a Glass Fibre/Epoxy composite system. An analytical model is proposed, in which the intact layers are divided into appropriate sub-layers for the stress components calculation. Knowing the SCF value at the tip of the crack, the possibility of fibres breakage in the adjacent layer is calculated using a statistical model, while the matrix failure is examined through a matrix failure criterion. SCF is recalculated taking into account the possible local stiffness reduction due to new modes of damage and the theoretical results are correlated with experimental findings.

1. INTRODUCTION

Once they were considered as exotic rare materials. Now, they have invaded into our everyday life increasing their market share. Polymeric composites show particular specific mechanical properties, while their design flexibility increases the designers' degrees of freedom. A third, equally important parameter is their ability to tolerate damage reflecting to their durability. In this context, the understanding of damage mechanisms and damage development during composite structures service life is of high importance regarding safety, social and economical impact. Load bearing capability of composite materials is the result of the precise collaboration between the reinforcing fibres and the matrix. The bulk polymeric materials show, in general, lower properties and are prone to early damage initiation under general thermo-mechanical loading. In transverse tension this damage mode, which is generally defined as matrix damage, is called intralaminar or transverse cracking and is comprised mainly by cracks within the constituent laminas.

Transverse cracking has been the subject of wide research during the last thirty five years and the results can be found in a large number of pertinent works. Several approaches and solutions have been applied to investigate the cracking initiation and growth and its effects on material behaviour. The approaches span the whole range from micromechanics to continuum damage mechanics [1-3]. In general, the damaged composite behaviour is modelled in these works through the degradation of global materials stiffness properties. Matrix cracking results in redistribution of the internal stress and strain state between the plies and each ply components, especially in the vicinity of cracks. Experimental studies have been conducted in order to quantify the stress and strain redistribution within a damaged composite by monitoring the local strains arising within the 0° layer of a general $[0°/\theta°]_s$ laminate due to cracking of the θ° layer, using a method based on Raman spectroscopy [4-6]. Raman spectroscopy utilizes the load sensitivity of Raman vibrational modes of crystalline fibres under mechanical loading, which is a result of the chemical bonds stiffness alteration under both extension and contraction. Since the focus spot of laser beam used and the sensor (fibre) is of the order of micrometer the spatial accuracy of the method provides a powerful tool to measure stresses and strain at the closest possible points to discontinuities like notches

and cracks [7-8].
Analytical modelling of the stress or strain state in cracked composites has been focused mainly on: (a) laminates thermoelastic properties reduction [9-11] and (b) the use of damage internal state variables to describe the damage evolution [1, 12]. The damage modes included transverse cracks and local delaminations at the cracks tip. While the success of those methods depends strongly on the accurate stress analysis, the interest in the stress distribution within the layer supporting the cracked lamina (-e) has been low. The most commonly used models like the shear-lag [12] and the Hashin's variational [13] models, do not calculate the stress concentration appearing at the crack front and the stresses redistribution in the intact laminae of a damaged composite is considered independent of the thickness coordinate. The foresaid stress concentration has been rendered by both experimental [7-8] and finite elements results, but only a few analytical models have been suggested to account for it [14].
In the present paper, a theoretical model is proposed to model the stress and strain distribution in a cracked cross-ply composite laminate. The model takes into account the secondary forms of damage arising within the intact layers adjacent to cracked ones. Secondary damage is located at a region close to the plies interface, thus the 0° layer is divided into a chosen number of sub-layers with reduced elastic properties attributed to this secondary damage. The elastic properties of the sub-layers are reduced corresponding to the damage state introduced in it during loading. Secondary damage modes are initiated by the stress concentration (SCF) at the crack tip which value is calculated. The damage is quantified using a statistical failure criterion regarding the fibres strength and a straight-forward failure criterion regarding the isotropic matrix material. The shape of the stress concentrations is described by functions with unknown shape parameters which are determined by minimizing the complementary energy of a repeating element of the laminate between two transverse cracks. The material under consideration is a glass fibres reinforced epoxy (GFRP) laminate. Theoretical SCF as a function of the distance from the crack tip is calculated, firstly assuming that the primary damage (90° layer matrix cracks) did not cause secondary phenomena and, following, for the case that transverse cracking led to new damage initiation within the adjacent layers. Next, by reducing each individual, or a combination, of layers properties, the modes of damage arising are identified and the stress concentration dependence on the various damage modes is revealed. Comparison between experimental results and theoretical model predictions demonstrates that, for the specific primary damage state, the specific secondary damage mode has been developed.

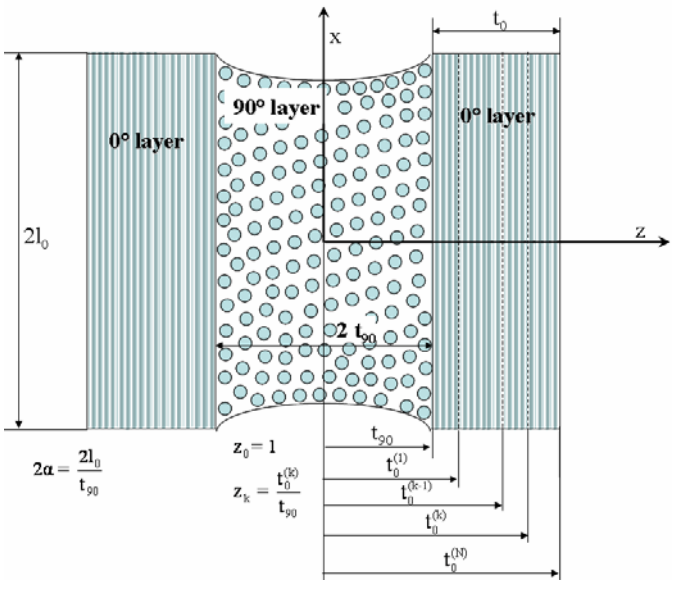

Figure 1: Geometrical characteristics of the repeating representative volume element.

2. MODELLING

2.1 Geometrical Description

A repeating element of length $2l_0$ between two transverse cracks in 90° layer of the laminate is considered, as shown in Fig. 1. Dimensionless normalized coordinates x, z are introduced by dividing them with t_{90}. The normalized crack spacing is $2a = 2l_0/t_{90}$. The 0° layer of thickness t_0 which supports the 90° layer of normalized half-thickness $z_0 = 1$ is assumed partially damaged and hence its elastic properties depend on the distance from the 0°/90° interface. In order to account for the properties degradation the 0° layer is divided into sub-layers with different elastic properties that are determined based on the rule that the properties reduction (i.e. degree of damage) is larger in sub-layers closer to the interface. Numbers are assigned to sub-layers, assigning the 90° layer k = 0. The sub-layers are numbered as k = 1, 2, …, N with k increasing with the distance from 0°/90° interface. The k-th sub-layer interface coordinates are denoted by z_k and z_{k-1}. The normalized coordinate of the outer surface is z_N. The sub-layer thickness is $t_0^{(k)} - t_0^{(k-1)}$.

2.2 Loading and Boundary Conditions

Loading consists of a thermal and a mechanical component. The mechanical part is an average far field stress σ_{x0}. The thermal component is the result of the mismatch between the thermal expansion coefficient and the temperature difference ΔT. At the outer boundary surface both normal and shear interlaminar stresses should be zero,

$$\sigma_{xz}^{N}\Big|_{z_N} = \sigma_{zz}^{N}\Big|_{z_N} = 0 \tag{1}$$

Upper index denotes the relevant sub-layer. Due to symmetry, interlaminar shear stress component on the mid-plane has to be zero,

$$\sigma_{xz}^{90}\Big|_{z=0} = 0 \tag{2}$$

Interlaminar shear stress continuity at both layers and sub-layers interfaces is written as:

$$\sigma_{xz}^{90}\Big|_{z=1} = \sigma_{xz}^{1}\Big|_{z=1}, \qquad \sigma_{xz}^{k}\Big|_{z_k} = \sigma_{xz}^{k+1}\Big|_{z_k}, \qquad k = 1, \ldots, N-1 \tag{3}$$

Out-of-plane interlaminar normal stress continuity is written as:

$$\sigma_{zz}^{90}\Big|_{z=1} = \sigma_{zz}^{1}\Big|_{z=1}, \qquad \sigma_{zz}^{k+1}\Big|_{z_k} = \sigma_{zz}^{k}\Big|_{z_k}, \qquad k = 1, \ldots, N-1 \tag{4}$$

Traction free conditions on crack surfaces are expressed by the form:

$$\sigma_{xx}^{90}\Big|_{x=\pm a} = \sigma_{xz}^{90}\Big|_{x=\pm a} = 0 \tag{5}$$

Finally, the integral force equilibrium has to be satisfied in any cross section $x = const$.
Since the stress problem is formulated in tractions, a method for stress determination is to use the principle of complementary energy minimization: the most accurate admissible stress state (stress components that automatically satisfy equilibrium equations and the formulated conditions in tractions (1) to (5)) is the one giving the lowest complementary energy. The particular shape of stress distribution is result of the minimization routine.

2.3 Stress Distributions

Equilibrium equations are automatically satisfied if the stresses corresponding to the 2-D problem described, are defined using the *stress function* as follows:

$$\sigma_{xx} = \frac{\partial^2 \Phi}{\partial z^2}, \qquad \sigma_{zz} = \frac{\partial^2 \Phi}{\partial x^2}, \qquad \sigma_{xz} = -\frac{\partial^2 \Phi}{\partial x \partial z} \tag{6}$$

For the 90°-layer the Φ is chosen to be in the form used in [14] that corresponds to Hashin's assumptions [13]

$$\Phi^{90} = \sigma_{x0}^{90}\left[\frac{z^2}{2} - \psi(x)\left(\frac{z^2}{2} + A^*\right)\right] \tag{7}$$

where, the $\psi(x)$ function should be determined. In (7) σ_{x0}^{90} is the macroscopic laminate (CLT) theory stress in the 90° layer. From (6) and (7) the stresses in the 90° layer are:

$$\sigma_{xx}^{90}=\sigma_{x0}^{90}\ \left[1-\psi(x)\right],\qquad \sigma_{zz}^{90}=-\sigma_{x0}^{90}\ \psi''(x)\ \left(\frac{z^2}{2}+A^*\right),\qquad \sigma_{xz}^{90}=\sigma_{x0}^{90}\ \psi'(x)\ z \tag{8}$$

According to the assumptions the axial stress in the 90° layer is independent on the z-coordinate. Consequently, the shear stress σ_{xz}^{90} varies linearly with z-coordinate, while σ_{zz}^{90} is parabolic. Thus the boundary condition (2) is automatically satisfied.

In the k-th sub-layer the shape of the complex stress components distributions along the z-coordinate is described by the initially unknown functions $\varphi_k(z)$:

$$\Phi^k=\sigma_{x0}^k\ \frac{z^2}{2}+\sigma_{x0}^{90}\ \varphi_k(z)\ \psi(x),\qquad k=1,\,2,\,\ldots,\,N \tag{9}$$

Here σ_{x0}^k is the CLT macroscopic stress in this sub-layer, while $\psi(x)$ and $\varphi_k(z)$ are functions to be determined. A similar approach just for one layer was used in [14]. Using equations (6) and (9) the stress components are given by:

$$\sigma_{xx}^k=\sigma_{x0}^k+\sigma_{x0}^{90}\varphi_k''(z)\psi(x),\quad \sigma_{zz}^k=\sigma_{x0}^{90}\varphi_k(z)\psi''(x),\quad \sigma_{xz}^k=-\sigma_{x0}^{90}\varphi_k'(z)\psi'(x) \tag{10}$$

The boundary conditions for the σ_{xz} (1) and (3) result in conditions for φ_k':

$$\varphi_N'(z_N)=0,\qquad \varphi_1'(1)=-1,\qquad \varphi_k'(z_k)=\varphi_{k+1}'(z_k),\qquad k=1,\,\ldots,\,N-1 \tag{11}$$

It can be shown that using functions which satisfy (11) the integral force equilibrium is automatically satisfied. Applying stress expressions (8) and (10) in (1) and (4) the following conditions are obtained:

$$\varphi_N(z_N)=0,\qquad \varphi_1(1)=-\frac{1}{2}-A^*,\qquad \varphi_k(z_k)=\varphi_{k+1}(z_k),\qquad k=1,\ldots,N-1 \tag{12}$$

The traction free boundary conditions at crack surfaces (5) lead to the following expression to be satisfied by the function $\psi(x)$:

$$\psi(\pm a)=1,\qquad \psi'(\pm a)=1 \tag{13}$$

2.4 Complementary Energy

The expression for complementary energy of a laminate element shown in Fig. 1 is:

$$V=U+2\ T\ \alpha_2\ \int_0^1\int_{-a}^{a}\left(\sigma_{xx}^{90}+\sigma_{zz}^{90}\right)\,dx\,dz+2\ T\sum_{k=1}^{N}\int_{z_{k-1}}^{z_k}\int_{-a}^{a}\left(\sigma_{xx}^k\ \alpha_x^k+\sigma_{zz}^k\ \alpha_z^k\right)\,dx\,dz \tag{14}$$

where, T is the service temperature, a_2, is the transverse thermal expansion coefficient of the unidirectional composite, and a_x and a_z are the thermal expansion coefficients of the 0° layer in x and z directions, respectively. U is the strain energy defined as:

$$U=2\int_0^1\int_{-a}^{a}W_{90}\,dx\,dz+2\sum_{k=1}^{N}\int_{z_{k-1}}^{z_k}\int_{-a}^{a}W_k\,dx\,dz \tag{15}$$

where

$$W_{90}=\frac{1}{2}\left\{\frac{\left(\sigma_{xx}^{90}\right)^2}{E_2}+\frac{\left(\sigma_{zz}^{90}\right)^2}{E_2}\right\}+\frac{1}{2}\left\{\frac{\left(\sigma_{xz}^{90}\right)^2}{G_{23}}-\frac{2\nu_{23}}{E_2}\ \sigma_{xx}^{90}\ \sigma_{zz}^{90}\right\} \tag{16}$$

$$W_k=\frac{1}{2}\left\{\frac{\left(\sigma_{xx}^k\right)^2}{E_1^k}+\frac{\left(\sigma_{zz}^k\right)^2}{E_2^k}\right\}+\frac{1}{2}\left\{\frac{\left(\sigma_{xz}^k\right)^2}{G_{12}^k}-\frac{2\nu_{12}^k}{E_1^k}\ \sigma_{xx}^k\ \sigma_{zz}^k\right\} \tag{17}$$

In (16) E_1, E_2, G_{23}, ν_{23} are the elastic constants of the 90° layer in local axes, while in

(17) E_1^k, E_2^k, G_{12}^k, v_{12}^k are the elastic constants of k-th sub-layer in its local axes.

The expressions for stresses given by (8) and (10) have to be substituted into the equations (14)-(17) and formally integrated over z (assuming that the shape of $\varphi(z)$ is known). Following the straightforward and tedious routine described in [14] the next expression of the complementary energy to be minimized is obtained:

$$V = V_0 + \left(\sigma_{\chi 0}^{90}\right)^2 \left\{ \int_{-a}^{a} \left[C_{00}\,\psi^2 + C_{02}\,\psi\psi'' + C_{22}\,(\psi'')^2 + C_{22}\,(\psi')^2 \right] dx \right\} \tag{18}$$

Constants C_{ij}, (i, j = 0, 1, 2) in (18) are defined as follows:

$$C_{00} = \sum_{k=0}^{N} I_1^k, \qquad C_{22} = \sum_{k=0}^{N} I_2^k, \qquad C_{11} = \sum_{k=0}^{N} I_3^k, \qquad C_{02} = \sum_{k=0}^{N} I_4^k, \qquad k = 0, 1, ..., N \tag{19}$$

In (19) I_i^0 (i = 1 – 4) depend on the assumed z-distribution of stresses in the 90° layer:

$$I_1^0 = \frac{1}{E_2}, \qquad I_2^0 = \frac{1}{E_2}\left(\frac{1}{20} + \frac{A^*}{3} + \left(A^*\right)^2 \right), \qquad I_3^0 = \frac{1}{G_{23}}, \qquad I_4^0 = -\frac{2\nu_{23}}{E_2}\left(\frac{1}{6} + A^* \right) \tag{20}$$

Constants I_i^k depend on the shape of stress distribution in the k-th sub-layer:

$$I_1^k = \frac{1}{E_1^k} \int_{z_{k-1}}^{z_k} \left[\varphi_k''(z)\right]^2 dz, \qquad I_2^k = \frac{1}{E_2^k} \int_{z_{k-1}}^{z_k} \left[\varphi_k(z)\right]^2 dz$$

$$k = 1, 2, ..., N \tag{21}$$

$$I_3^k = \frac{1}{G_{12}^k} \int_{z_{k-1}}^{z_k} \left[\varphi_k'(z)\right]^2 dz, \qquad I_4^k = -\frac{2\nu_{12}^k}{E_1^k} \int_{z_{k-1}}^{z_k} \varphi_k(z)\,\varphi_k''(z)\,dz$$

2.5 Solution of the Stress Distribution Problem

Function which minimizes equation (18) has to satisfy the differential equation [13]:

$$C_{22}\,\psi'''' + \left(C_{02} - C_{11}\right)\psi'' + C_{00}\,\psi = 0 \tag{22}$$

and the boundary conditions given by (13). The solution for C_{ij} values corresponding to polymer matrix composites is of the form:

$$\psi = A_1\,\cosh(\alpha x)\cos(\beta x) + A_2\,\sinh(\alpha x)\sin(\beta x) \tag{23}$$

In (23)

$$A_1 = \frac{2\,\alpha\,\cosh(\alpha a)\sin(\beta a)}{\alpha\,\sin(2\beta a) + \beta\,\sinh(2\alpha a)} + \frac{2\,\beta\,\sinh(\alpha a)\cos(\beta a)}{\alpha\,\sin(2\beta a) + \beta\,\sinh(2\alpha a)} \tag{24a}$$

and

$$A_2 = \frac{2\,\beta\,\cosh(\alpha a)\sin(\beta a)}{\alpha\,\sin(2\beta a) + \beta\,\sinh(2\alpha a)} - \frac{2\,\alpha\,\sinh(\alpha a)\cos(\beta a)}{\alpha\,\sin(2\beta a) + \beta\,\sinh(2\alpha a)} \tag{24b}$$

Parameters α and β are calculated by the following expressions:

$$\alpha = q^{1/4}\cos\left(\frac{\theta}{2}\right), \qquad \beta = q^{1/4}\sin\left(\frac{\theta}{2}\right) \tag{25a}$$

where

$$\tan(\theta) = \sqrt{\frac{4q}{p^2} - 1} \tag{25b}$$

while constants p and q depend on the C_{ij} constants by the following expressions

$$p = \frac{C_{02} - C_{11}}{C_{22}}, \qquad q = \frac{C_{00}}{C_{22}} \tag{26}$$

The solution (23)-(26) corresponds to the minimum of complementary energy in the framework of the used assumptions. This minimum value is given by [14]

$$V_{min} = V_0 + 2\left(\sigma_{x0}^{90}\right)^2 C_{00} \frac{2\alpha\beta}{\alpha^2+\beta^2} \cdot \frac{\cosh(2\alpha a) - \cos(2\beta a)}{\alpha \sin(2\beta a) + \beta \sinh(2\alpha a)} \quad (27)$$

As one can see the solution is based on the z-dependence of stresses given by functions $\varphi_k(z)$ which until now are arbitrary. Even the numerical value of the minimum complementary energy (27) depends on this choice. This situation which seems rather voluntary is actually reduced to the possibility to find the best distribution $\varphi_k(z)$ by comparing the values of the energy minima. Taking different $\varphi_k(z)$ will result in different solutions (given by the same functional form (23) with different values of V_{min} (27)). The one which gives lowest value is the best. Thus the minimization becomes an optimization process.

There is an infinite number of ways how to choose $\varphi_k(z)$. The accuracy of the results depends on the success in finding forms that are physically justified. In this work, shape functions with arbitrary numerical parameters were chosen, which insure that the stress concentration is decreasing with the distance from the crack tip. The exponential decay of the stress concentration factor with the distance from the stress singularity source led to the choice of a function that includes an exponential term. The rate of decrease is characterized by parameters which are to be determined in the minimization routine. The shape functions used in this study are

$$\varphi_k(z) = B_k \frac{(z - z_{k-1})^2}{2} + D_k \exp\left(-\Delta_k (z - z_{k-1})\right) \quad (28)$$

Using these exponential shape functions the solution and also the minimum value of the complementary energy V_{min} depends on values of Δ_k for $k = 1, \ldots, N$

$$V_{min} = f(\Delta_1, \Delta_2, \ldots, \Delta_N) \quad (29)$$

Analytical iterative methods can be used to find the set of Δ_k for k = 1, 2, …, N which gives the lowest value and hence the most exact solution.

Table 1 Mechanical Properties of the undamaged layers

0°	E_1 **(GPa)**	E_2 **(GPa)**	G_{12} **(GPa)**	ν_{12}
	43	13	4.69	0.3
90°	E_1 **(GPa)**	E_2 **(GPa)**	G_{23} **(GPa)**	ν_{23}
	43	13	4.58	0.42 [15]

3. RESULTS AND DISCUSSION

3.1 Stresses Distributions

The presented analytical model was applied to determine the stress state at the crack tip of a cracked cross-ply GFRP laminate. In the first calculation the 0-layer properties were the same in all positions. Nevertheless in order to keep the same model at all steps the 0° layer was divided into two sub-layers. The initial sub-layer interface was introduced at z where experimental SCF [7] almost takes the value 1. Thus the first sub-layer thickness, t_1, was 0.075 mm while the second, t_2, was 0.565 mm. Applying the boundary and continuity conditions, a set of 2N+2 linear equations are formed for N sub-layers. The unknown constants resulting from the shape function (28) are 3N+1. Thus a total of N-1 constants should be determined using an iterative process based on the principle of complementary energy minimization. In the described problem this corresponds to a system of 6 equations for 7 unknowns. Thus the complementary energy minimization is used for the determination of 1 of the unknowns. As a first step no secondary damage is

assumed, thus both sub-layers are considered with the same mechanical properties of the undamaged 0° ply. The undamaged properties for both plies are presented in Table 1. The crack density is 0.1 cracks/mm and the corresponding applied strain [7] is 0.54%. The v_{23} value of the lamina isotropic 2-3 plane was calculated by the semi-empirical model proposed in [15].

The resulting SCF corresponding to the longitudinal stress, σ_{xx}, as a function of the distance along the z-axis of the laminate is presented in Fig. 2. The z-distance is normalized with respect to the 90° layer thickness for calculation purposes. The maximum SCF value is predicted to be about 8 at distance z = 1 (plies interface), which is typical for this type of materials isotropy. The application of two sub-layers in this step does not give any additional information, since no secondary damage is introduced and the SCF distribution is the same, independent of the layer thickness used. It is the same as in the model with only one layer. A rapid decay of the SCF with increasing z-distance is observed. Strain is reaching the external applied strain value at a normalized distance of 0.05.

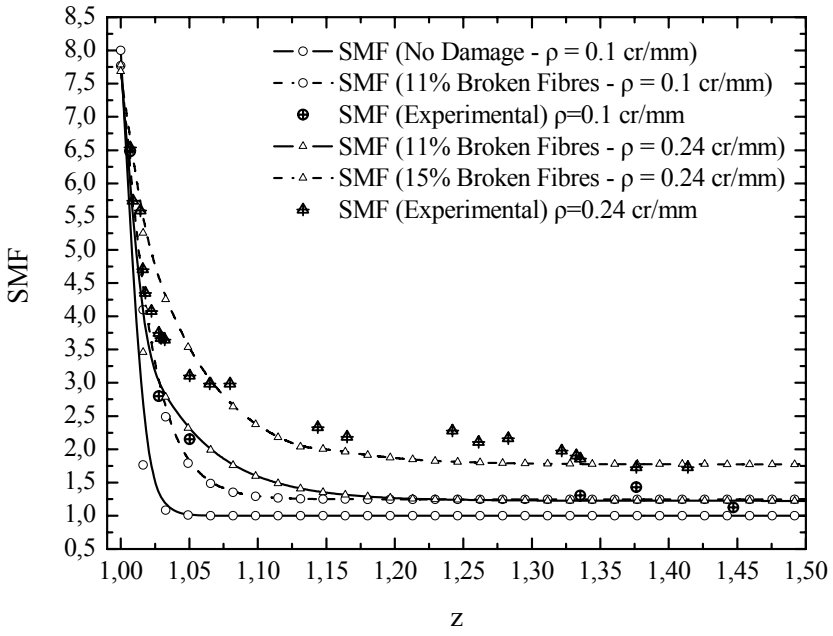

Figure 2: Stress distributions as a function of the z-distance along the ply thickness. Theoretical model predictions against experimental data.

Theoretical model predictions are compared with experimental data from the literature [7]. The experimental data are presented in Fig. 2. The experimental data show a smoother decay than theoretical. This implies that secondary damage has been introduced into the 0° ply. The nature and the amount of secondary damage is examined in next section.

3.2 Damage Identification – SCF Correction – Verification

Fibres tensile strength is highly dependent on the presence of sub-microscopic voids on their surface that act as stress concentrations. These voids are known as "Griffith's cracks" [16] and they are treated in a statistical manner. Weibull distribution of the fibres tensile strength is generally accepted as a quite accurate approximation [17]. In this study the two-parameter Weibull distribution is considered to estimate the amount of broken fibres in the vicinity of the crack tip. The distribution function is written in the form:

$$F(x;b,c) = 1 - exp\left[-\left(\frac{x}{b}\right)^{c}\right], \qquad b \geq 0,\ c \geq 0 \tag{30}$$

In equation (30) *F(x;b,c)* represents the probability that the fracture strain is equal to or less than *x*. *b* is the Weibull scale parameter and c is the Weibull shape parameter, which are determined experimentally for each fibre material. In the present study the Weibull parameters values are taken from the literature for E-Glass fibres with 25mm gage length [18] and are equal to: *b*=5.81% and *c*=15. We use the actual strain at the vicinity of the crack as *x* in (30). Since $\varepsilon_{xx} = K\,\varepsilon_a$, where ε_a is the external applied strain (ε_a = 0.54% [7]) and *K* is the SCF as given by the model and shown in Fig. 2, the following equation is obtained, which will give the probability for the fibres to fail:

$$F(\varepsilon_{xx};b,c) = 1 - exp\left[-\left(\frac{K\varepsilon_a}{b}\right)^c\right], \qquad b \geq 0,\ c \geq 0 \tag{31}$$

Since the SCF is a function of z- coordinate, a distribution of the *F* probability as a function of *z* could be drawn. This distribution for the considered crack density ρ = 0.1 cracks/mm is presented in Fig. 3.

As expected, the fibres probability to failure is high in the region adjacent to the crack front, while it reduces as the z-distance increases and practically diminishes at a *z* of about 0.03 from the plies interface. For the modelling needs it is conservative to assume that due to the cracking of the 90° ply the percentage of broken fibres within the 0° ply over a distance 0.05 from the plies interface (Fig. 3, crossed hatched area) is equal to the average *F*. This hypothesis results in an amount of 11% broken fibres.

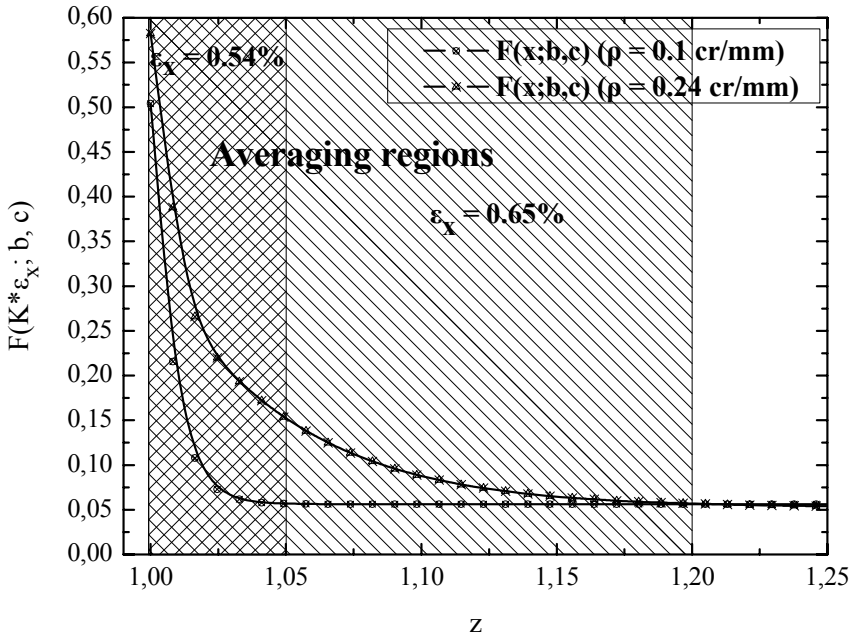

Figure 3. Distribution of the fibres probability to failure as a function of z-distance

The other secondary damage mode which could be present in the 0° ply is matrix related and depends on its strength. In order to investigate possible matrix related failures (yielding, splitting, delaminations, etc) a straight-forward comparison between the matrix strength and the actual strain at the crack tip is done. A typical value of the strain to failure ε_m^* for epoxy resins is of about 3-4%. The actual tensile strain at the region before the crack front is, as explained earlier, $K\varepsilon_a$ which, if averaged in the pre-described region, results in a value of ε_x = 0.97% which is too small to cause significant matrix damage.

Collecting this information that is based on the model predictions for the SCF values at the region ahead of the crack tip, a recalculation will be performed in order to include the thus determined secondary damage modes. Sub-layers thicknesses are selected based on the principle that their boundary is at the point where SCF becomes 1. Thus in this

recalculation the sub-layers boundary is at z = 1.05. Longitudinal Young's Modulus, E_1, that is mostly dependent on the fibres, will be reduced by 11% in the first sub-layer of size 0.05 since this is the broken fibres percentage calculated. The material properties related to the matrix, transverse and shear Moduli and Poisson's ratios will remain unchanged since the matrix proved to remain intact. A recalculation of the SCF distribution along the z distance is performed using the modified material properties. The results are presented in Fig. 2. Comparing the theoretical predictions with the experimental data, a satisfactory fitting is observed. It is, therefore, concluded that the presented method based on the proposed model and the described determination of possible secondary damage results in good predictions.

Now SCF and secondary damage modes predictions procedure will be repeated in order to examine the approach to find the laminate stress and secondary damage state at a higher transverse crack density level. Extracting data regarding the experimental SCF and crack density values from the literature [11] the state of ρ = 0.24 cracks/mm at an applied strain level of ε_a = 0.65% is chosen. SCF distribution as a function of z is calculated following the same process, first taking into account the secondary damage calculated at the previous step (11% broken fibres). The SCF distribution thus derived is shown in Fig. 2. As expected it follows similar path as the SCF distribution calculated at before, although with variations caused by the different crack density. The corresponding experimental data are also shown in Fig. 2. A significantly higher deviation between the theoretical predictions and the experimental data is observed. As before, this deviation is attributed to the secondary damage modes further development, which is going to be estimated in the next.

Using equation (31) where applied strain is ε_a = 0.65% [11] and the SCF values are taken from Fig. 2, the distribution of F probability as a function of the z is constructed as shown in Fig. 3. The probability for fibres fracture is similar at z = 1 while reduces less rapidly than in the previous case and diminishes after z= 1.2. Averaging the probability over the hatched region (from z = 1 to z = 1.2) a possibility of 18% broken fibres is obtained.

Possible matrix damage is again investigated through the comparison between the new average $K\varepsilon_a$ from z= 1 to z= 1.2 and ε_m^*= 3-4%. Average $K\varepsilon_a$ gives a value of 1.36%, which again is smaller than ε_m^*. Thus, the only damage mode present is fibres breakage at a percentage of 15%, which is represented by a E_1 reduction of the same amount. Using the new data regarding the materials properties and the sub-layers boundary, which at this point should be at z = 1.2, SCF distribution is recalculated and the results are presented in Fig. 2. A better approximation of the experimental data is achieved, while the difference may be explained by the fact that the 0° layer has been divided only into two sub-layers. Optimization is possible, but this would significantly increase the complexity of the procedure.

4. CONCLUSIONS

An analytical model is proposed for the determination of the secondary damage modes initiating in cross-ply composite laminate with transverse cracks. The 0° layer is divided into a certain number of sub-layers with varying mechanical properties corresponding to the extent of secondary damage. The lowest elastic properties are assigned to the sub-layer adjacent to the 0°/90° interface. The shape of the stress concentrations is described by functions with unknown shape parameters. These parameters are determined by an iterative complementary energy minimization process. The secondary damage modes arising due to cracking are directly estimated using the theoretical predictions for the stress concentration factor (SCF) assuming no damage in 0-layer and applying the SCF in a statistical model for prediction of the broken fibres percentage and in a straight-forward comparison to the matrix strength for investigation of possible matrix damage.

The thus found modes of damage are introduced into the SCF calculation by reduction of the corresponding material properties in the damaged zone. A corrected SCF distribution along the thickness of the laminate is determined. Theoretical predictions are compared to experimental data with a satisfactory agreement. That means that the proposed procedure can predict well secondary damage modes and their effect on the material behaviour which could be useful in damage tolerance design.

REFERENCES

1- Talreja, R. *"Damage characterization by internal variables"*. In: Pipes, R.B. and Talreja, R., editors. *Damage mechanics of composite materials*. Composite materials series, vol. 9. Amsterdam: Elsevier; 1994.

2- Varna, J., Joffe, R., Akshantala, N.V. and Talreja, R. "Damage in composite laminates with off-axis plies", *Composites Science & Technology*, 1999; 59(14): 2139-2147.

3- Kashtalyan, M. and Soutis, C. "Analysis of Composite Laminates with Intra- and Interlaminar Damage", *Progress in Aerospace Sciences*, 2005; 41(2): 152-173.

4- Parthenios, J., Katerelos, D. G., Psarras, G. C. and Galiotis, C. "Aramid fibres: a multifunctional sensor for monitoring stress/strain fields and damage development in composite materials", *Engineering Fracture Mechanics*, 2002; 69(9): 1067-1078.

5- Katerelos, D. G., McCartney, L. N. and Galiotis, C. "Local strain re-distribution and stiffness degradation in cross-ply polymer composites under tension", *Acta Materialia*, 2005; 53(12): 3335-3343.

6- Katerelos, D. T. G., Lundmark, P., Varna, J. and Galiotis, C. "Analysis of matrix cracking in GFRP laminates using Raman spectroscopy", *Composites Science & Technology*, 2007; 67(9): 1946-1954.

7- Katerelos, D. G. and Galiotis, C. "Axial strain redistribution resulting from off-axis ply cracking in polymer composites", *Applied Physics Letters*, 2004; 85(17): 3752-3754.

8- Katerelos, D. T. G. and Galiotis, C. *"Experimental Determination of Stress Concentrations in Composite Laminates and their Effects on Damage Evolution"*. In: *Applied Mechanics and Materials*, vols. 5-6, Trans Tech Publications, Switzerland; 2006.

9- Kashtalyan, M. and Soutis, C. "Mechanisms of internal damage and their effect on the behavior and properties of cross-ply composite laminates", *International Applied Mechanics*, 2002; 38 (6): 641-657.

10- Gudmundson, P. and Zang, W. "A universal model for thermoelastic properties of macro-cracked composite laminates", *International Journal of Solids and Structures*, 1993; 30(23): 3211-3231.

11- Lundmark P. and Varna J., "Constitutive Relationships for Laminates with Ply Cracks in In-plane Loading", *International Journal of Damage Mechanics* (2005); 14 (3); 235-261.

12- Lim, S. G., Hong, C. S. "Prediction of transverse cracking and stiffness reduction in cross-ply laminated composites", *Journal of Composite Materials*, 1989; 23(7): 695-713.

13- Hashin, Z. "Analysis of cracked laminates: a variational approach", *Mechanics of Materials*, 1985; 4(2): 121-136.

14- Varna, J. and Berglund, L. A. "Multiple Transverse Cracking and Stiffness Reduction in Cross-Ply Laminates", *Journal of Composites Technology & Research*, 1991; 13(2): 97-106.

15- Philippidis, T. P. and Theocaris, P. S. "The Transverse Poisson's Ratio in Fiber Reinforced Laminae by Means of a Hybrid Experimental Approach", *Journal of Composite Materials*, 1994; 28(3): 252-261.

16- Philips, L. N. (Ed.) "*Design with Advanced Composite Materials*", UK, The Design Council, Springer-Verlag; 1989.

17- Dirikolu, M. H., Aktas, A. and Birgoren, B. "Statistical Analysis of Fracture Strength of Composite Materials using Weibull Distribution", *Turkish Journal of Engineering and Environmental Sciences*, 2002; 26: 45-48.

18- Brown, E. N., Davis, A. K., Jonnalagadda, K. D. and Sottos, N. R. "Effect of Surface Treatment on the Hydrolytic Stability of E – Glass Fiber Bundle Tensile Strength", *Composites Science and Technology*, 2005; 65(1): 129-136.